

# Versatile Microfluidics Separation of Colloids by Combining External Flow with Light-Induced Chemical Activity

Marek Bekir,\* Marcel Sperling, Daniela Vasquez Muñoz, Cevin Braksch, Alexander Böker, Nino Lomadze, Mihail N. Popescu, and Svetlana Santer\*

Separation of particles by size, morphology, or material identity is of paramount importance in fields such as filtration or bioanalytics. Up to now separation of particles distinguished solely by surface properties or bulk/surface morphology remains a very challenging process. Here a combination of pressure-driven microfluidic flow and local self-phoresis/osmosis are proposed via the light-induced chemical activity of a photoactive azobenzene-surfactant solution. This process induces a vertical displacement of the sedimented particles, which depends on their size and surface properties. Consequently, different colloidal components experience different regions of the ambient microfluidic shear flow. Accordingly, a simple, versatile method for the separation of such can be achieved by elution times in a sense of particle chromatography. The concepts are illustrated via experimental studies, complemented by theoretical analysis, which include the separation of bulk-porous from bulk-compact colloidal particles and the separation of particles distinguished solely by slight differences in their surface physico-chemical properties.

## 1. Introduction

The very active area of research on manipulation of small objects (nano/micro-scaled) emerges out of the growing importance of micro- and nano-technology as a key field offering revolutionary solutions for fields such as novel sensor designs, developing strategies for self-healing complex and integrated structures, or the creation of new materials realizing lattice plasmon engineering, quantum aggregates, or hybrid bio-electro-mechanical systems.<sup>[1–5]</sup> In these research fields, objects such as active colloids, metallic clusters, or functional protein complexes ranging from a few micrometers down to less than 10 nm are thought of differently nowadays: Instead of large ensembles of constituents forming an effective media, single elements constitute complex structures and assemblies on the

length scale of their own size. For this, individual selection and sorting of desired small particles concerning size, surface morphology, and composition are of great importance.<sup>[6]</sup>

Currently, there are two general approaches for the separation and sorting of micro- and nano-sized objects: On the one hand, there are conventional methods such as chromatography,<sup>[7]</sup> cross-flow<sup>[8]</sup> and dead-end<sup>[9]</sup> filtration, while on the other hand, there are the more recently developed microfluidics-based approaches.<sup>[10]</sup> The latter have several advantages over the conventional methods as they can address small amounts of sample volume in a short time and simultaneously addressing single objects out of a heterogeneous ensemble is nowadays possible.<sup>[11,12]</sup> The physical principles of operation employ the unique characteristics of microscale flow phenomena, where particle size dependent forces, such as the shear gradient lift and the wall lift force induce lateral migration of particles toward dedicated streamlines between the channel centerline and channel walls.<sup>[6,13–15]</sup> The destination flow line of a colloidal particle is sensitive to both its size and its elasticity; consequently, various fractionation principles, such as pinched flow fractionation<sup>[16]</sup> or deterministic lateral displacement,<sup>[17]</sup> can be implemented.<sup>[18–20]</sup>


If, however, the particles do not differ in size, but solely in chemical composition, surface morphology, roughness, or porosity, microfluidic separation and filtration become a near impossible task and no well-established methods exist. Recent investigation demonstrates a separation of quantum dots over optical properties using plasmonic thin-layer

M. Bekir, D. V. Muñoz, C. Braksch, N. Lomadze, S. Santer  
Institute of Physics and Astronomy  
University of Potsdam  
Karl-Liebknecht Str. 24/25, 14476 Potsdam, Germany  
E-mail: marek.bekir@uni-potsdam.de; santer@uni-potsdam.de

M. Sperling, A. Böker  
Fraunhofer Institute for Applied Polymer Research IAP  
Geiselbergstraße 69, 14476 Potsdam-Golm, Germany

M. N. Popescu  
Department Theory of Inhomogeneous Condensed Matter  
Max-Planck-Institut für Intelligente Systeme  
Heisenbergstr. 3, 70569 Stuttgart, Germany

M. N. Popescu  
Física Teórica, Department Theory of Inhomogeneous Condensed Matter  
Universidad de Sevilla  
41080, Apdo. 1065 Sevilla, Spain

 The ORCID identification number(s) for the author(s) of this article can be found under <https://doi.org/10.1002/adma.202300358>

© 2023 The Authors. Advanced Materials published by Wiley-VCH GmbH. This is an open access article under the terms of the Creative Commons Attribution-NonCommercial License, which permits use, distribution and reproduction in any medium, provided the original work is properly cited and is not used for commercial purposes.

DOI: 10.1002/adma.202300358

chromatography.<sup>[21]</sup> Another possible avenue to follow toward this aim is that of exploiting the principles of phoresis, a transport mechanism that is intrinsically effective at the microscale and sensitive to the surface properties of the particles; such an approach has been successfully illustrated in ref. [22], where cross-stream salt gradients have been used to induce the deflection of colloidal particles as they move downstream in a microfluidic channel. The advantages of phoretic phenomena come, on the other hand, with the caveat that creating and maintaining steady-state gradients of suitable thermodynamic variables over length scales much larger than the size of the particles remains very challenging. An option, which bypasses the requirement of externally maintained thermodynamic gradients, is to induce the motion of colloidal particles by combining the phoretic response, which is surface-type sensitive, with gradients that are locally induced.

The recently reported phenomenology of light-driven diffusioosmosis (LDDO) in which local flows are generated at a solid/liquid interface that involves a solution containing a photo-responsive surfactant by illumination with light of a suitable wavelength, is a particularly versatile method to achieve this.<sup>[23]</sup> The photo-responsive surfactant employed carries an azobenzene group within its hydrophobic tail and can undergo a reversible photo-isomerization reaction from a more stable *trans*- (hydrophobic) to a metastable *cis*- (more hydrophilic) conformation.<sup>[24–28]</sup> Under the irradiation of a localized region of the surface with, for example, ultraviolet UV light, the photo-isomerization of the surfactant molecules generates a gradient in the *cis*- and *trans*-isomers at the interface, which induces diffusioosmotic (DO) flow.<sup>[29–33]</sup> The direction of the DO flow depends on the irradiation wavelength, because this controls the relative imbalance between the two isomers, while its amplitude depends on the intensity of the light. Thus, the DO flow can be easily adjusted by tuning irradiation parameters.<sup>[34]</sup> The same phenomenon is responsible for the generation of local light-driven diffusioosmotic flow (*l*-LDDO) at/by a small object that can effectively adsorb one of the isomers.<sup>[35]</sup> In this case, under uniform irradiation with light particles loaded with *trans*-isomers become a source of a laterally inhomogeneous excess of *cis*-isomers that diffuse out of particles, which leads to an effective concentration gradient and a corresponding *l*-LDDO flow. It has been shown that the strength, duration, and direction of the process strongly depend on the irradiation wavelength (at fixed intensity) due to the different kinetics of photo-isomerization at the surface as compared to the same process in the bulk solution.<sup>[36,37]</sup> For example, under irradiation with blue light at which in a photo-stationary state both isomers are present in solution, the DO flow is continuous over the whole irradiation time. Under exposure to UV light, the flow is transient and decays when the particles empty their load of *cis*-isomers.<sup>[38]</sup> Such local DO flow can, thus, be generated at any surface absorbing *trans*- and repelling *cis*-isomers;<sup>[39]</sup> examples here are porous particles,<sup>[35]</sup> microgels,<sup>[40]</sup> hair, nails, wood sticks, sand, soil, etc.<sup>[41]</sup>

In this work, we show that by combining the chemical activity-controlled *l*-LDDO with a pressure-driven flow within a channel, it is possible to achieve the separation of micron-sized particles sedimented at the channel wall. The asymmetry in the environment of the particle, due to the presence of the wall, induces a displacement of the particle in the direction normal to the

wall when the chemically active *l*-LDDO is induced. Accordingly, when the particles are exposed simultaneously to an ambient hydrodynamic shear flow and illumination of a suitable wavelength, the particles explore a different region of the flow than the one probed in the absence of the illumination. Thus, they will be moving downstream at a speed slower (or faster) than the one when the illumination is absent. Experiments, and complementary theoretical analysis, show that the magnitude of the displacement along the direction normal to the wall, and thus the change in velocity upon illumination, depends both on the size of the particle, due to the interplay with the sedimentation tendency, as well as on the surface properties of the particles. The wavelength of the illumination controls the relative imbalance of isomers and, hence, the nature of the *l*-LDDO flow. Consequently, mixtures of particles of either the same material but different sizes, or similar in size but differing in surface properties (different materials, or plain vs porous particles) can be effectively separated by making use of a suitable light wavelength to achieve significantly different elution times, that is, a working similar to that of chromatographic devices. This versatile and powerful separation method is illustrated by several proof-of-concept experimental realizations. In particular, for the case of — otherwise difficult to separate — mixtures of same-size porous and plain particles, we show that the increase in velocity upon illumination is much stronger for the porous colloids (up to 5 times), which ensures a very efficient separation.

## 2. Results and Discussion

The colloidal particles can generate *local*-LDDO flow upon illumination with light of a suitable wavelength when dispersed in an aqueous solution of the azobenzene-containing photo-sensitive surfactant. A manifestation of this “chemical activity” phenomenon is that of the formation of regions depleted of tracers around immobilized porous particles (alternatively, at different wavelengths of the illumination the tracers collapse into crystalline structures around the immobilized particles).<sup>[35]</sup> This observation suggests that a spherical particle immersed in the aqueous solution of the photo-sensitive surfactant (the chemical formula of which is shown in Figure 1b) and sedimented near a wall will experience an effective repulsion (or attraction), depending on the details of the system (see also the discussion in ref. [35]) as well as Section 4.3.2 of the Theoretical Model part of the Experimental Section and the Section S4.1 of the Supporting Information). The effective interaction between an active particle and the wall is the combined effect of: i) the particle moving in the direction normal to the wall by diffusiophoresis due to the inhomogeneous distribution of *cis* surfactant molecules in that direction (an example is provided by Figure S6b, Supporting Information) and ii) the particle being carried by (drifting with) the osmotic flow induced by the inhomogeneous distribution of *cis* surfactant molecules along the wall. Accordingly, if the particle is not immobilized, then we expect to see that it changes its mechanical equilibrium distance from the wall. This expectation can be tested, as we discuss below, by exposing the particles to an external shear flow and looking for a change in the drift velocity of the particles upon turning on the chemical activity via illumination. Assuming it holds, the active elevation of particles of similar sizes but different morphologies or different surface properties will

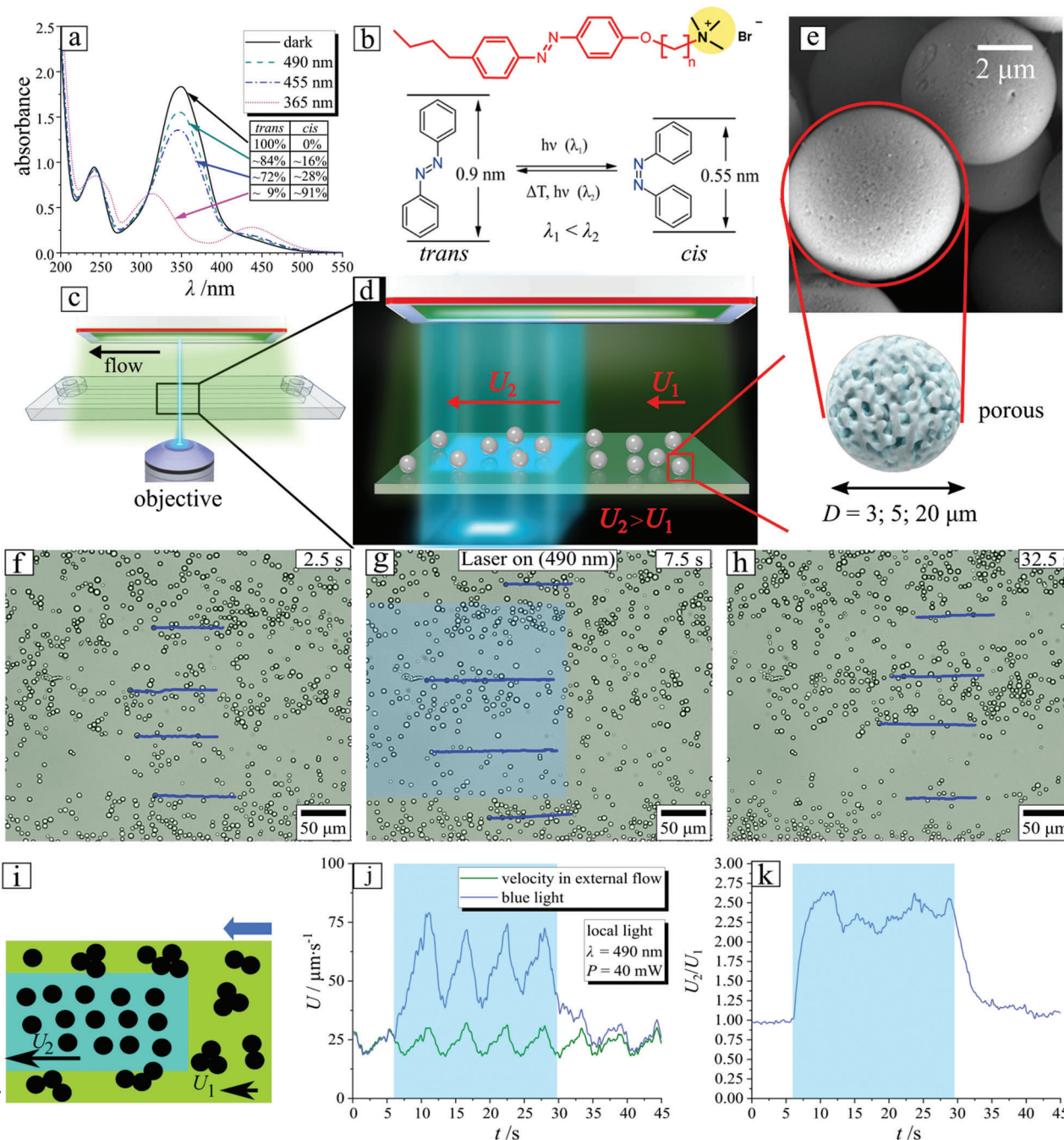


**Figure 1.** a) UV-vis absorption spectra of photo-sensitive surfactant at photo-stationary state under irradiation with different wavelengths as indicated in the legend. The inserted table depicts the corresponding ratios of *trans* and *cis* isomers. b) Chemical structure of the surfactant and the two isomers of the azobenzene group. c) Schematics of the fluid cell and d) scheme of the zoomed area;  $U_1$  and  $U_2$  are the particle velocities in the dark and under illumination with blue light, respectively. The colloids are sedimented at the bottom of the chamber. e) SEM micrograph of the porous particle of 5  $\mu\text{m}$  in diameter; a schematic drawing of the particle is inserted below. f-h) Optical micrographs of colloidal particles moving from the right to the left over the illuminated area (blue rectangular in (i)) at different times: f) 2.5 s, g) 7.5 s, and h) 32.5 s; the illumination is turned on at  $t_1 = 6$  s and off at  $t_2 = 30$  s, respectively. The corresponding video is provided in Video S2 (Supporting Information). i) Schematics indicating the monitored area; the velocity,  $U_2$ , of the particles within the illuminated area (blue rectangle) is larger than the one,  $U_1$ , outside it. j) Mean velocity as a function of time: the blue curve indicates the velocity of the particles passing through the illuminated area (of  $\approx 75\,000\ \mu\text{m}^2$ ) ( $\lambda = 490\ \text{nm}$ ,  $P = 40\ \text{mW}$ ), while the green line shows the velocity of the particles not passing through that region. The cyan region indicates the time interval during which the blue light is on. k) The ratio  $U_2/U_1$  of the velocities of the two types of trajectories as a function of time. The cyan region indicates the time interval during which the blue light is on. The average sample size of particles per frame in the analyzed area is  $124 \pm 7$  particles.

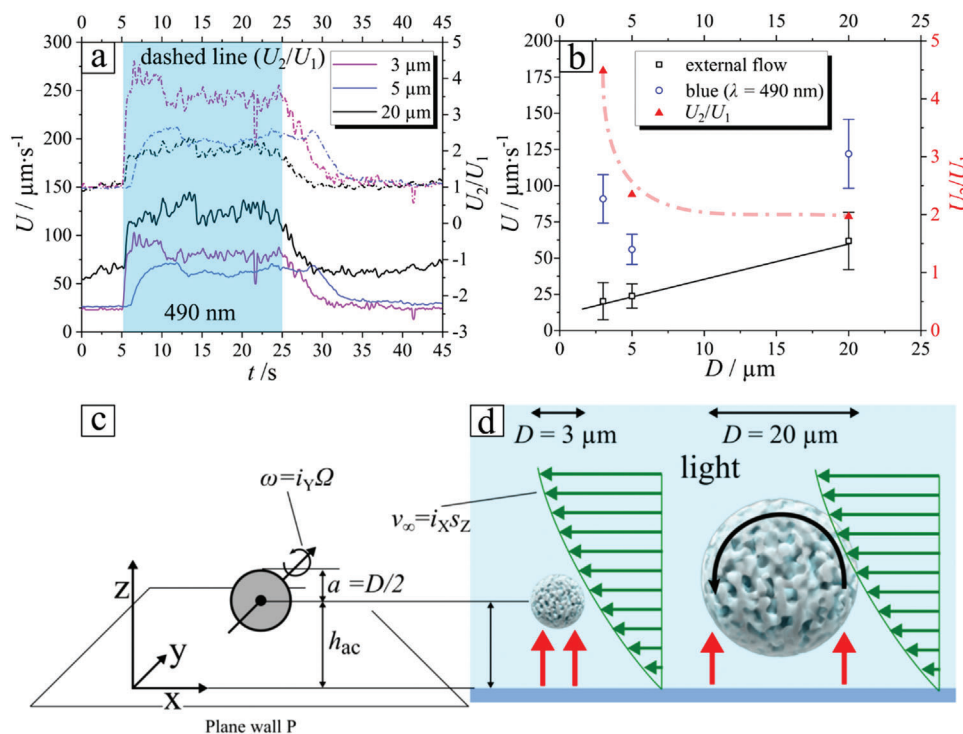


**Figure 2.** a) Averaged particle velocity as a function of time for colloidal particles of three different diameters as indicated in the legend. The meanings of the cyan region and of the ratio  $U_2/U_1$  are the same as in Figure 1. b) Average velocity as a function of particle diameter in the absence of illumination (black line) and within the illuminated region (blue data points); the “normalized velocity”  $U_2/U_1$  as a function of the particle diameter  $D$ . Red dashed line is for eye guiding. The corresponding videos are provided in Supporting Information, Videos S2–S4 (Supporting Information). c) Geometry of the particle near a surface. d) Schematic representation of lift off of the porous particle in a laminar flow (green arrows) from a surface under blue light irradiation. The case shown here corresponds to the chemical-activity-induced hydrodynamic flow lifting the particle into a higher focal plane. Error bars calculated using the standard deviation. The average sample size of particles  $n$  per frame is  $141 \pm 9$ ,  $124 \pm 7$ , and  $8 \pm 3$  for 3, 5, and 20  $\mu\text{m}$  large diameters, respectively.

differ. This is the fact because the kinetics of the isomerization reaction depends on the nature of the particle (porous or plain) and the transduction of chemical inhomogeneities into particle-wall, while effective interaction depends on the morphology and material identity of the surface of the particle. This can be exploited, in combination with a pressure-driven flow, to efficiently sort same-size particles, exhibiting different bulk/surface properties, within a microfluidics device via well-separated elution times.

We turn to the experimental verification of our hypothesis that the chemical activity leads to potentially significant changes in the elevation of the sedimented particles. We demonstrate this by using porous silica particles (pore size of  $\approx 6$  nm, BET porosity value =  $850 \text{ m}^2 \text{ g}^{-1}$ ) with diameters  $D$  ranging between 0.5 and 20  $\mu\text{m}$  (Figure 1e for the particles of 3, 5, and 20  $\mu\text{m}$  and Figure S2, Supporting Information for all sizes in the range above) dispersed in an aqueous solution of the photo-sensitive surfactant ( $c_{\text{azo}} = 1 \text{ mM}$ ) within a microfluidic chamber (length: 1 cm, thickness: 0.5 cm, height: 0.5 mm, Figure 1c). The chamber is connected to a peristaltic pump, which enables a continuous pumping of the surfactant aqueous solution through the chamber and, thus, provides the pressure-driven shear flow that drifts the particles along the channel. Using video microscopy the velocity of each particle is determined from their tracked trajectories, and an average velocity is computed over the ensemble (Figure 1f–h,

Video S1, Supporting Information). Within the channel we select an area of rectangular shape which is then illuminated by a laser (wavelength 490 nm,  $P = 40\text{--}50 \text{ mW}$ ) (Figure 1d); at this wavelength (blue light) the ratio of the *trans/cis* isomers at a photo-stationary state is 84%/16%, respectively (Figure 1a).<sup>[42]</sup> At these parameters, we expect a repulsive interaction between the active particles and the wall, and thus a “lift-off” of the particles, manifested as an increased drift velocity, as they pass the illuminated area.

This is indeed the case, as can be seen in Figure 1f, which shows an example of porous particles ( $D = 5 \mu\text{m}$ ) moving along the glass surface within a pressure-driven flow of volumetric flow rate  $dV/dt \approx 200 \mu\text{L min}^{-1}$ . In the areas that are not illuminated, the average particle velocity is  $23.5 \mu\text{m s}^{-1}$  (see Video S1, Supporting Information). When the laser light ( $\lambda = 490 \text{ nm}$ ,  $P = 40 \text{ mW}$ ) is switched on, the velocity in the illuminated area increases by a factor of  $\approx 2.5$  times (Figure 1g,k); switching off the light leads to the decrease in mean velocity of the particles back to the initial value (Figure 1h), which shows that the process is reversible. The oscillation which is observed superimposed over the average value is the effect of the pressure variations of the peristaltic pump (Figure 1j). By using particles of various sizes, we further can infer that the effect depends on the size of the particle as illustrated in Figure 2 (see also Figure S2a,b, Supporting Information).

**Table 1.** Summary of the experimental data for the active particles (first three columns), the calculated hovering heights for the active particles  $h_{ac}$  assuming an illumination of 490 nm. (Equation (4) see Section 4.3.1 of the Theoretical Calculations (Experimental Section)) and the corresponding changes relative to the case of inert particles.  $a$  particle radius,  $U$  particle velocity,  $U/a$  normalized particle velocity against the radius,  $h_{ac}$  hovering height,  $\Delta h$  difference of  $h_{ac}$  and  $a$ .

$a$	$U$	$U/a$	$h_{ac}$	$\Delta h = h_{ac} - a$	$h_{ac}/a$	$\Delta h/a$
[ $\mu\text{m}$ ]	[ $\mu\text{m s}^{-1}$ ]	[ $\text{s}^{-1}$ ]	[ $\mu\text{m}$ ]	[ $\mu\text{m}$ ]		
1.5	$90 \pm 17$	60	5.8	4.3	3.9	2.9
2.5	$56 \pm 11$	22	3.9	1.4	1.6	0.6
10.0	$122 \pm 24$	12	10.6	0.6	1.1	0.1

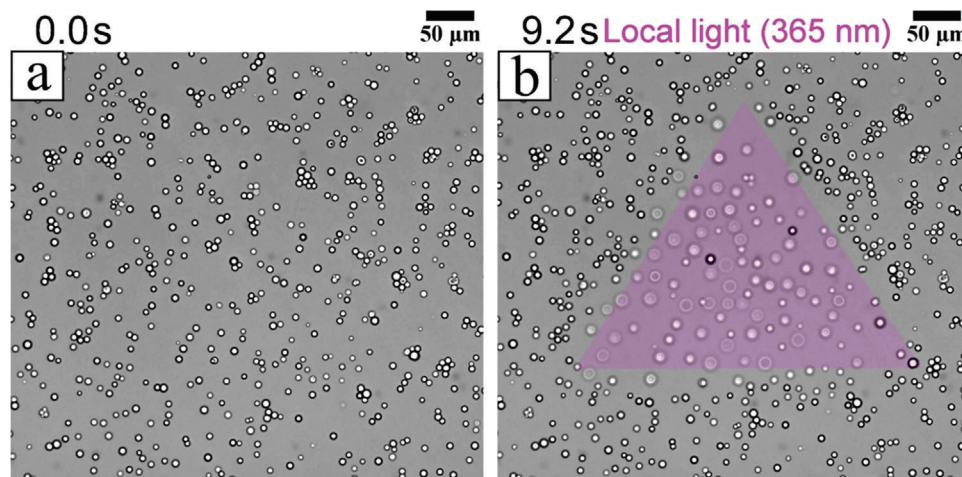


**Figure 3.** a) Snapshot of optical micrograph of the porous particles before illumination and b) during exposure to modulated light spot ( $\lambda = 365 \text{ nm}$ ,  $I = 120 \text{ mW cm}^{-2}$ ) from Video S8. The hovering of the particles in the triangle-shaped illuminated area results in out-of-focus imaging. The external flow is switched off.

The linear dependence of the velocity in the non-illuminated areas on the size of the particle is in agreement with the expectation that the motion we observe is the drift by the pressure-driven flow.<sup>[45]</sup> As discussed in the Section: Theoretical Models and Analysis, from this dependence one estimates a rate of shear  $S \approx 15.5 \text{ s}^{-1}$ , which is in excellent agreement with the value of  $\approx 15 \text{ s}^{-1}$  calculated from the flow rate in the microchannel (Section S3 of the Supporting Information). Assuming that for the active particles the observed velocity is also the drift by the pressure-driven flow, one can use the results from ref. [45] to extract the height  $h_{ac}$  (Figure 2c,d) and the change  $\Delta h = h_{ac} - h \approx h_{ac} - a$  above the wall at which the active particles are located (see Experimental Section, Section: Theoretical Models and Analysis). The results (Table 1) are compatible both with the direct observation by microscopy of the shifts out of the focus (see below) and with the theoretical estimates (Section S2 of the Supporting Information) based on a simple model, discussed in the Methods (Section: Theoretical Models and Analysis), for a lift due to activity-induced local-LDDO.

The direct observation of the lift-off is carried out in the absence of external flow by illuminating only a specific region of the surface, here a triangle-shaped area as shown in Figure 3. The particles move out of the focus (as shown in Figure 3b) during hovering, which is larger for UV light in comparison to the one under blue light illumination, and light-intensity dependent (see Video S7, Supporting Information irradiation with  $\lambda = 455 \text{ nm}$

and  $\lambda = 365 \text{ nm}$  Video S8, Supporting Information). The larger elevation height under irradiation with UV light results in a more enhanced velocity of the particles exposed to external flow (see Videos S9,S10, Figure S3, Supporting Information recorded for particles of 3 and 5  $\mu\text{m}$  in diameter, respectively). Note that particle-particle repulsive interactions resulting in ordering at the irradiated area (similarly to recently reported results in ref. [43]) are also present, but not directly visible in Figure 3b, since the particles elevate out of the focus.

In the following, we propose a mechanism for the separation of particles of equal size but different surface morphology/roughness by taking advantage of the particle illumination-induced hovering. To demonstrate this, we expose a binary mixture of plain and porous particles of the same size to external flow and study their velocity under illumination with light of blue wavelength (Figure 4). To differentiate between the particles, the fluorescein dye (Figure 4b, excitation in blue range at 494 nm and emission at 512 nm) is added to the sample. The anionic fluorescein forms aggregates (micelles) with cationic surfactant and since the porous particles have larger surface area, more dye is accommodated allowing to distinguish particles in fluorescence signal. Indeed, in transmission mode the particles appear similar in external flow (Figure 4c,d), while under irradiation with blue light the porous particles are brighter and, simultaneously, they are faster than the plain ones (Figure 4e,f). We recall that the surfactant molecules adsorb also on the surface of plain silica

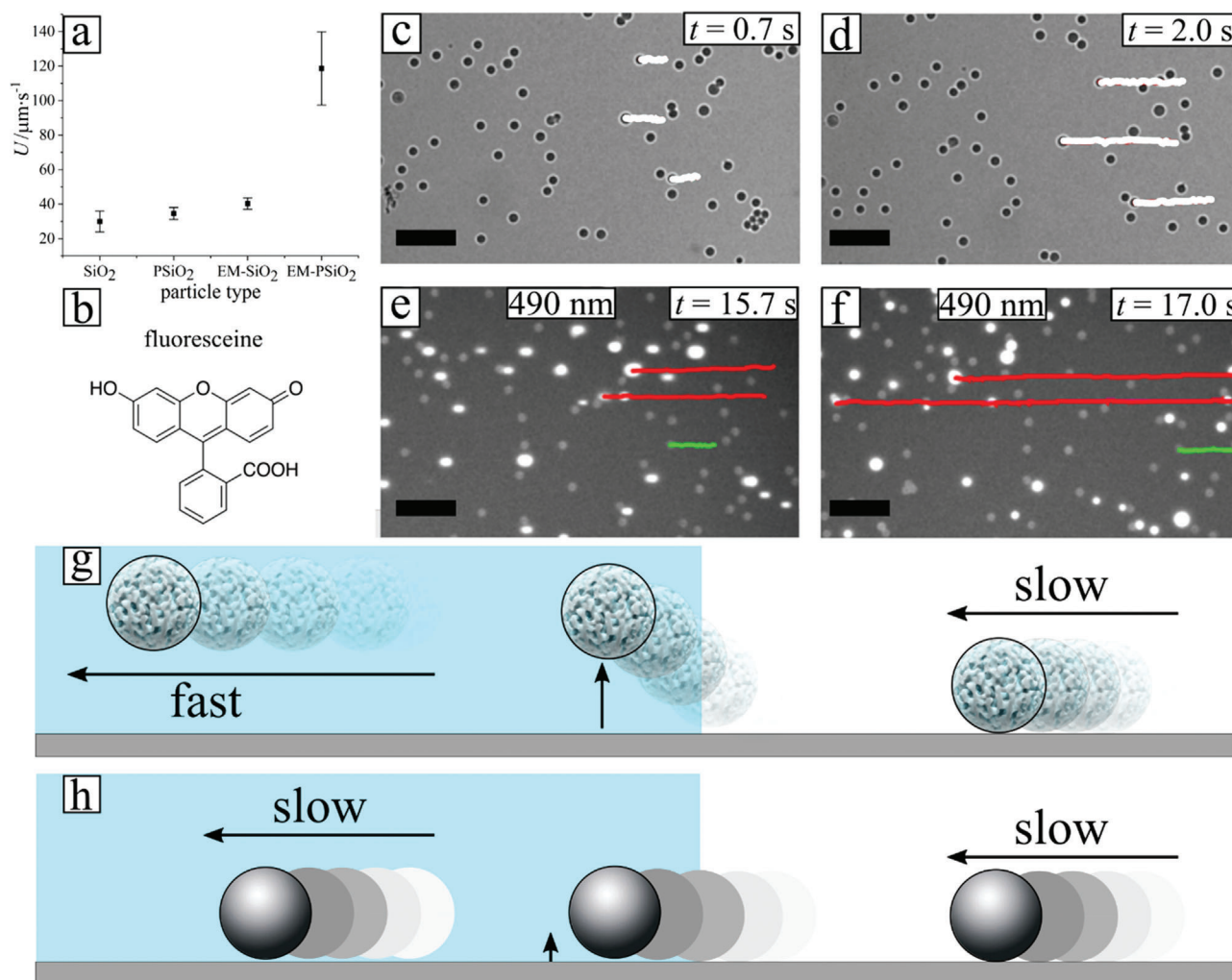


**Figure 4.** a) Mean velocity  $U$  (from trajectories tracked over 30 s) of  $\text{SiO}_2$  (plain particles) and  $\text{P-SiO}_2$  (porous particles) in transmission (no illumination) and emission mode (denoted in EM,  $\lambda = 490$  nm,  $I = 55$  mW  $\text{cm}^{-2}$ ). b) Chemical structure of fluorescein dye. Snapshots of the optical micrographs taken c,d) in transmission mode (no illumination) and e,f) fluorescence signal taken in emission mode (blue illumination). The trajectories are recorded over a time interval of 2 seconds, where a representative snapshot is displayed at  $t = 0.7$  and 2 s (+15 s for emission signal). The trajectories of several colloids are marked in red (porous) and green (plain) to illustrate the extent of the particle motion in the micrograph area. The scale bar (black rectangle) is 20  $\mu\text{m}$ . The corresponding video is provided in Video S11 (Supporting Information). g,h) Scheme of the separation process. The porous particles are lifted off in the illuminated area and thus are exposed to the range of larger velocities of the shear flow (g), than the plain particles (h). Solution pH has a value of 6. Sample size is 30 particles. Error bars calculated using standard deviation.

particles. Thus the *local*-LDDO flow is generated at the non-porous colloids as well, however, the extent of flow and the lift-off tendency is usually significantly less pronounced, and consequently the change in drift by the external flow is much smaller (almost negligible in many cases).

The analysis of the velocity change shows that only porous particles are “accelerated” under illumination ( $\lambda = 490$  nm,  $P = 50$  mW); the corresponding velocity ratio  $U_2/U_1$  reaches values up to 2.5 (Figure S4, Videos S12,S13, Supporting Information). In this way, the porous particles will arrive at a given downstream destination significantly faster than the plain ones, and thus they can be collected and separated out of the mixture at different times.

This phenomenon is not specific solely to the case of porous versus plain particles; it is manifest as well when dealing with

particles of the same size but different surface coatings. This is demonstrated by using porous particles ( $D = 5$   $\mu\text{m}$ ) having a different surface coating, that is, hydroxy ( $-\text{OH}$ ) and amino ( $-\text{NH}_2$ ) groups. When they are illuminated with blue light ( $\lambda = 490$  nm) (Figure 5a, Video S14, Supporting Information), one observes that the velocity of the negatively charged particles (grey line in Figure 5a) is larger than that of those having positively charged surface (blue line, Figure 5a).

Our approach to particle separation is applicable for other types of colloids, too. For instance, polystyrene particles show also different increase in velocity under illumination depending on the surface coating (see Figure 5b, Video S15, Supporting Information). In this case, illumination with UV light is found to lead to a more effective separation than illumination with blue light (see also Figure S5, Supporting Information). This is most

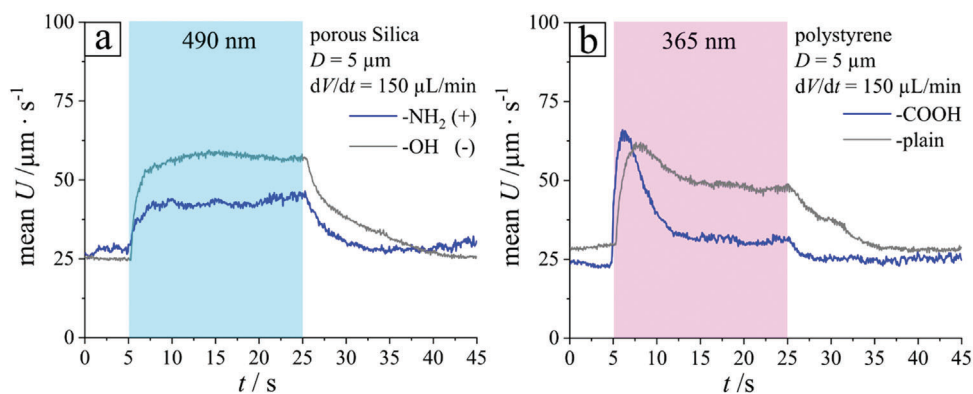


**Figure 5.** a) Mean velocity of porous silica particles having different surface charges: positively charged due to amino terminated surface (blue line) and negatively charged due to hydroxyl-enriched coating (grey line). The particles are exposed to an external flow of volumetric velocity  $150 \mu\text{L min}^{-1}$ , and illuminated with blue light during the time interval between 5 and 25 s (illustrated by the colored box). b) Similar dependency for the polystyrene particles of different coating: carboxyl-enriched (blue line) and plain surface (grey line). Polymeric samples were immersed 1 day in a photosensitive surfactant solution. The illumination in this case is performed with UV light, which here provides better results than the illumination with blue light. The light is collimated globally from the top with an intensity  $I = 11.5 \text{ mW cm}^{-2}$ . Solution pH has a value of 6. The average sample size per frame is for a)  $-\text{OH } 188 \pm 35$ ;  $-\text{NH}_2 \ 173 \pm 15$ ; b) plain  $116 \pm 16$ ;  $-\text{COOH } 238 \pm 30$ .

likely the result of either a different kinetics of isomerization of the photo-responsive surfactant inside of pores of different materials, or of a different pore structure for the PS particles compared to the silica ones, or both. Summarizing: The data in Figures 2, 4, and 5 suggests a very versatile method for the separation of a large variety of particle types, which offers the means to design, for example, surface-sensitive separation technologies.

We demonstrate that already a short illumination of a binary mixture (1:1) of dye-labeled  $P\text{-SiO}_2$  and non-labeled  $\text{SiO}_2$  of equally sized particles ( $D \approx 5 \mu\text{m}$ ) allows for effective separation (see Video S16, Figure S9, Supporting Information Section S5). Much better separation might be achieved under longer operation time, where the most challenging part will be a precise collection of two individual fractions at different times.

### 3. Conclusion

We have observed a light-triggered increase in the velocity of porous colloidal particles immersed in a photosensitive surfactant solution and exposed to external hydrodynamic flow. The mechanism is based on the particles becoming chemically active and lifting off (hovering) when illuminated; the hovering of the particle is the result of local diffusioosmotic flow generated at the colloid during the photo-isomerization of the azobenzene-containing surfactant molecules present in solution. The lift-off tendency depends on the surface morphology of the dispersed particles, is most pronounced for particles of smaller diameter, and the total lift can be as large as the diameter of the particle itself; accordingly, the relative velocity gain under light stimulation can be very significant. By exploiting this feature, we have demonstrated that a binary mixture of two types of particles similar in size and surface chemistry but differing in overall surface area (compact and porous silica particles) can be effectively separated by elution times via the increase in the speed of the porous particles under illumination. Furthermore, this effect is also suitable for separating plain from coated particles, as demonstrated for porous silica with two different coatings as well as for plain

versus coated polymeric particles. Overall, this new discovery provides a versatile, simple, and swift method for separating colloidal particles of the same size and distinguished only by differences in their surface morphology or material composition, which is very desirable, for instance, in purifying a heterogeneous particle ensemble with respect to a surface modification (such as, e.g., increase in roughness or porosity, attachment surface functionalization, thin polymer or protein layer, etc.).

### 4. Experimental Section

**Materials:** The azobenzene-containing trimethyl-ammonium bromide surfactant ( $\text{C}_4\text{-Azo-OC}_6\text{TMB}$ ) was synthesized as described elsewhere.<sup>[44]</sup> The surfactant (Figure 1b) consisted of a spacer of 6 methylene groups between the positively charged trimethyl-ammonium bromide head group and the azobenzene unit with a butyl tail attached. Water (Milli-Q system) with a specific resistance larger than  $18 \text{ M}\Omega \text{ cm}$  was used to prepare aqueous solutions. Figure 1a shows characteristic UV-vis absorption spectra of the surfactant recorded at photo-stationary state under exposure to light of different wavelengths. The *trans*-isomer (denoted as dark) had a characteristic absorption band ( $\pi\text{-}\pi^*$  transition) with a maximum at 351 nm. The spectrum of the *cis*-isomer was characterized by two absorption bands with maxima at 313 nm ( $\pi\text{-}\pi^*$  transition) and 437 nm ( $n\text{-}\pi^*$  transition). The lifetime of the metastable *cis*-isomer in dark or in red light ( $\lambda = 625 \text{ nm}$ ) was  $\approx 48 \text{ h}$  at  $23 \text{ }^\circ\text{C}$ .

Meso Porous silica colloids of different diameters  $D$  otherwise unmodified, ranging between 0.5 and  $20 \mu\text{m}$ , and non-porous silica colloids of  $D = (4.0 \pm 0.24) \mu\text{m}$  were purchased from Micromod and micro-Particles GmbH (Germany). Meso-porous silica colloids of average  $5 \mu\text{m}$  diameter with amino functionalization ( $-\text{NH}_2$ ) were purchased from the company Micromod. Polystyrene particles with diameter  $D = (5.0 \pm 0.10) \mu\text{m}$  either with a plain or carboxy surface functionalization ( $-\text{COOH}$ ) were purchased from micro-Particles GmbH (Germany).

The aqueous dispersion of colloids was mixed with surfactant stock solution at a concentration of 1 mM and equilibrated at least for 24 h before measurements. A microfluidic flow chamber  $\mu\text{-slide}^{\text{VI}}$  with a glass bottom coverslip (Ibidi GmbH) of a volume of  $40 \mu\text{l}$  was used in order to provide a closed environment. When an aqueous dispersion of azobenzene containing surfactant and porous or non-porous silica colloids was placed in a chamber, the colloids sediment down to a glass surface. The chamber was connected to a continuous pumping system with either a peristaltic pump

(IPC peristaltic pump, Ismatec) or a syringe pump (PHD ultra, Harvard Apparatus). All samples were kept in dark or in red light to prevent unwanted photo-isomerization. The measurements were conducted at room temperature of  $T = 23\text{ }^{\circ}\text{C}$ .

**Methods:** An inverted microscope Olympus IX73 equipped with a light source of various wavelengths was used for the measurements. The global illumination from the top side was performed with LED lamps of different wavelengths: green ( $\lambda = 532\text{ nm}$ , M530L4) or red LED ( $\lambda = 625\text{ nm}$ , M625L1-C1 (Thorlabs GmbH)). Local illumination from the bottom side of the sample proceeded either with laser light (490 nm, Thorlabs GmbH) or with SLM operating with blue LED lamps ( $\lambda = 455\text{ nm}$ , M455D2, Thorlabs GmbH).

The illumination power was directly measured at the sample position prior to each measurement using an optical power meter PM100D with a sensor S170C (Thorlabs GmbH, Germany). The intensities between 0.2 and 20 mW cm<sup>-2</sup> were applied in experiments. The increase of the temperature of the surfactant solution during irradiation with laser power used in this study ( $P = 40\text{--}50\text{ mW}$ ) was  $\approx 0.2$  and  $0.2\text{ }^{\circ}\text{C}$  for UV and blue light, respectively.

Time-resolved micrographs were recorded with a CCD camera (Hamamatsu ORCA-Flash4.0 LT (C11440)) at 30 frames per second.

SEM micrographs were recorded with a commercial ZEISS ULTRA PLUS-40-61 microscope.

**Data Analysis:** Recorded videos were decomposed into single-frame images and converted to grayscale. Each image then was subjected to particle detection involving contour extraction using a series of three thresholding steps. The first two steps referred to brightness thresholding in order to separate the background from particles. In the resulting transformed image, particle contours were detected and thresholded by their area in terms of a min-max interval assumed within the particle range. This was done to exclude arbitrary artificial object detection. Using the as-identified contours, the center of mass was calculated for each object, which further served as location coordinates.

From the as-prepared frame images, object tracking occurred via retrieval of the minimum distance object within the next frame. This led to the identification of each individual particle trajectory as well as its frame-to-frame velocity by multiplying the traveled distance with the frame-rate, and the particle radius. Further analysis was done twofold. First, histograms as well as mean and median velocities observed from frame to frame, including the standard deviation (see Statistical Analysis Section), were calculated. The difference in the behavior of the median and mean thereby allowed for the detection of potential biases affecting the mean due to extreme outliers. Second, the mean velocity of each particle over its complete trajectory was then correlated to its size (diameter). Analysis was done via Python software using several software packages: Bokeh, NumPy, OpenCV-python, Matplotlib, Openpyxl, Pandas, and SciPy.

**Statistical Analysis:** Time-resolved average velocity  $\bar{U}$ : The sample size  $n$  (number of particles) of individual velocity  $U_i$  for each frame-to-frame were averaged using the arithmetic mean to obtain  $\bar{U}$ :

$$\bar{U} = \frac{1}{n} \left( \sum_{i=1}^n U_i \right) \quad (1)$$

and corresponding standard deviation  $\sigma$  calculated from the square root of the variance for the sample size of  $n-1$ :

$$\sigma = \sqrt{\frac{1}{n-1} \sum_{n=i} (U_i - \bar{U})^2} \quad (2)$$

All data were treated without evaluation of outliers.

The particle-velocity histograms were calculated with Equation (1), where the arithmetic mean particle velocity  $\bar{U}$  per particle size was calculated from all momentum velocities  $U_i$  (frame-to-next frame) of one entire trajectory crossing the image containing  $n$  number of frames.

Statistical analysis was done via Python software using several software packages: Bokeh, Numpy, OpenCV-python, Matplotlib, Openpyxl, Pandas, and SciPy.

Histogram velocities were binned using the software Origin with software package 2D frequency count binning. For the radii  $a_i$  the binning size center step was adjusted to  $1.0\text{ }\mu\text{m}$  with a minimum binning begin at  $0.5\text{ }\mu\text{m}$  and maximum binning end  $15\text{ }\mu\text{m}$ . For the velocities  $U_i$  the binning size center step was adjusted to  $10\text{ }\mu\text{m s}^{-1}$  with a minimum binning begin at  $10\text{ }\mu\text{m s}^{-1}$  and a maximum binning end of  $140\text{ }\mu\text{m s}^{-1}$ . Error range was calculated binned data range.

**Calculation of the Height Above the Wall from the Measured Drift Velocities:** The observed velocities were interpreted within the textbook theoretical framework provided by the ref. [45] (see also Figure 2c,d). This was possible because the particles were heavy and their size was much smaller than the dimensions of the microfluidic channel; accordingly, the particles explored only a limited region, near the wall, of the pressure-driven flow, for which an approximation by a linear shear flow was well justified.

In the absence of light (inert particles), the sedimentation of the porous silica particles led to an equilibrium separation from the wall  $\delta = h - a$  (Figure 2c), which was set by the balance of the apparent (i.e., corrected for buoyancy) weight and the DLVO forces (here mainly the electrostatic double-layer repulsion). The expectation, based on the results reported in the many available Surface Force Apparatus and Atomic Force Colloidal Microscopy studies of silica or glass in water systems, was that  $\delta \leq 100\text{ nm}$ . Accordingly, for the particles of radii  $a = 1.5, 2.5,$  and  $10\text{ }\mu\text{m}$ , respectively, one had  $\delta/a \leq 0.07$  and therefore  $h \approx a$ . This was the so-called "lubrication regime", for which one could write the approximation (stemming from the more complex result in ref. [45] under the observation that the  $\delta/a$  term in our case is irrelevant):<sup>[45]</sup>

$$U \approx \frac{1}{2} S \cdot a \quad (3)$$

where  $S$  is the shear rate. In brief: in the lubrication regime, the drift velocity is given by ref. [45] as  $U \approx \frac{0.7431}{0.6376 - 0.2 \ln(\frac{\delta}{a})} S \cdot h$ . For  $\delta$  in the order of  $100\text{ nm}$  and radii  $a$  in the range of  $1.5$  to  $10\text{ }\mu\text{meters}$ , as in the experiments, the factor  $\delta/a$  was expected to be at least  $0.001$  and at most  $0.07$ . In this range of values, the numerical factor  $A$  (the whole expression in the form of  $S h$ ) was equal to  $1/2$  plus a small correction which depended on the radius  $a$ . Accordingly, for the sake of simplicity in the first approximation the correction term was disregarded and we set  $A = 1/2$ . Note that for a linear shear flow the quantity  $(S a)$  represents the velocity of the unperturbed flow evaluated at the center of the particle; thus, the intuitive interpretation of Equation (3) is that the velocity of the particle exposed to the flow was half of that of the unperturbed flow at the location of the center of the particle. The linear dependence of  $U$  on particle radius  $a$ , was compatible with the behavior observed experimentally (black squares, Figure 2b). From the slope of a linear fit to the data in Figure 2b one arrives at  $S \approx 15.5\text{ s}^{-1}$ , which is in excellent agreement with the value of  $15\text{ s}^{-1}$  independently evaluated from the flow rate and the geometry of the channel (see Section S3 of the Supporting Information). This provided a good cross-check for the validity of the lubrication regime approximation.

The velocity-size histogram analysis of a mixture of porous particles of different diameters measured in a time range of  $10\text{ s}$  from Video S5 (Supporting Information) ( $t = 0\text{--}10\text{ s}$ ) and Video S6 (Supporting Information) ( $t = 30\text{--}40\text{ s}$ ) confirmed a linear increase of the velocity with the diameter (Figure S2a,b, Supporting Information).

When the particles were illuminated (i.e., the particles become chemically active), an additional effective force started acting on them, which would lead to a displacement of the vertical position of mechanical equilibrium to a new height  $h_{ac}$  (see Figure 2c). The expectation, based on the previous experimental studies that reported a repulsive interaction for such particles and on the observed increase in the drift velocity of the particles, was that the displacement was towards larger heights. In this case, the lubrication approximation did no longer hold; however, one could progress



by using the asymptotic expression, in principle valid for  $h \gg a$ , to obtain the approximation<sup>[45]</sup>

$$\frac{U}{a} \approx S \cdot \frac{h_{ac}}{a} \cdot \left[ 1 - \frac{5}{16} \cdot \left( \frac{a}{h_{ac}} \right)^3 \right] \quad (4)$$

With  $S$  known from the fitting, Equation (4) provided the means for the conversion of the experimentally measured values  $U$  to the values  $h_{ac}$  of the heights above the wall (and the corresponding lift values  $\Delta h = h_{ac} - h \approx h_{ac} - a$ ), provided in Table 1.

It was noted that in these experiments the Reynolds number  $Re$  corresponding to the pressure-driven flow of the aqueous solution (density  $\rho = 10^3 \text{ kg m}^{-3}$ , viscosity  $\mu = 10^3 \text{ Pa s}$ ) within the microfluidic channel of height  $h \approx 1 \text{ mm}$  with velocity  $V \approx 1 \text{ mm s}^{-1}$  was estimated to be at most  $Re = \rho V h / \mu \approx 1$ . (The characteristic velocity scale  $V \approx 1 \text{ mm s}^{-1}$  followed from the known flow rate and the dimensions of the channel, see Equation (S5), Supporting Information). Accordingly, a word of caution is in order, in that the use of the results in ref. [45] (which was carried out under the assumption of Stokes flow, that is, zero Reynolds number) for extracting the height at which the particles drifted in the pressure-driven flow was a somewhat borderline approximation.

**Theoretical Model of the Chemical Activity of the Porous Particles and Estimates of  $h_{ac}$ :** Theoretical Model: Here it was tried to estimate theoretically the lift-off height of the porous, chemically active particles. A simple model was used within the framework of self-diffusiophoresis with electrically neutral solutes. Under illumination with light of a suitable wavelength, the azobenzene molecules present in the *trans*-state (hydrophobic) in the solution, as well as within the pores of the particles, underwent a conformation change to the *cis* state (hydrophilic) (because the silica is basically transparent for most of the wavelengths of interest in this work).<sup>[42]</sup> For the particles, the *cis* surfactant was expelled from the pores (which initially, i.e., before illumination, were filled solely with *trans* molecules), while *trans* molecules from the surrounding solution were absorbed back within the pores. Accordingly, the surfactant solution within the pores might reach a non-trivial steady-state (i.e., the pores were not completely emptied of the *trans* surfactant) in contact with the bulk surfactant solution; this indeed was the case for the illumination of blue light. In particular, when blue light (wavelength,  $\lambda = 455 \text{ nm}$ ) was used, a steady state of the surfactant in the solution emerges in which the *cis* and *trans* isomers were both presented in a 1:3 ratio.<sup>[42]</sup>

Therefore, the porous particles effectively acted as sinks/sources of *trans/cis* molecules, respectively; that is, in a first approximation, in which these in and out fluxes were assumed to be uniform over the surface, it was a model chemically active particle with a "uniform flux"  $K$  boundary condition at its surface.<sup>[46]</sup> When such an active particle was in the vicinity of a wall, which was a reflecting boundary for the species in the solution, the densities of *cis* and/or *trans* molecules varied along the surface of the particle as well as along the surface of the wall. The gradients along the surface for the densities of each of the two isomers gave rise to the actuation of the fluid around the particle and along the wall (Figure S8, Supporting Information). This process was approximated by a phoretic slip, at each location on the surface of the particle or of the wall, proportional to the local gradient of that species. The coefficient (phoretic-mobility)  $b_i$ , which connected the phoretic slip to the gradient in the density of the species "i", depended on the molecular species and on the material properties of the surface. While in general the phoretic mobility of a rough surface (porous particle) was expected to be different from that of a smooth surface (non-porous particle), here such details were neglected and simply assumed that the connection between the density gradients and the phoretic slip is the same as that for a smooth surface. Furthermore, in the following one disregards the gradients of the *trans* molecules. The argument is that the concentration of *trans* molecules in the solution is constant above CMC, and their molecular diffusion is fast enough, so that the local "consumption" (i.e., absorption into the pores of a particle) induces only very small, negligible changes from the "bulk" value, even when the particle was not far from a wall. Accordingly, at this stage, the model chemical activity of the porous particle involved only the number density  $C(\mathbf{r})$  of the *cis* molecules,

which were released by the particle uniformly over its surface with a rate  $K$  and diffused with diffusion constant  $D_{\text{diff}}$  into the surrounding solution of bulk density  $c_\infty$ . Fast diffusion of the molecular species, and a small Péclet number for their transport (i.e., transport by diffusion dominates the one by fluid advection) was assumed such that  $C(\mathbf{r})$  could be taken to be relaxed to the corresponding steady-state around the particle at rest at its current location. Thus,  $C(\mathbf{r})$  was governed by the Laplace equation,  $\nabla^2 C(\mathbf{r}) = 0$  with the boundary conditions above,<sup>[47]</sup> that is  $C(|\mathbf{r}| \rightarrow \infty) \rightarrow 0$ ,  $\mathbf{n} \cdot (-D \nabla C(\mathbf{r})) = K$ , at the surface of the particle, and  $\mathbf{n} \cdot (-D \nabla C(\mathbf{r})) = 0$ , at the wall (where  $\mathbf{n}$  denotes the inner normal of the corresponding surface). In this regard, the relevant hierarchy of the time scales was that of the short time of the relaxation by diffusion of the molecular *cis* monomers around the particle releasing them and the long time of the motion of the particle. The former was estimated as  $a^2/D \approx 10^{-2} \text{ s}$ , for particles of micrometer radius  $a$  and a diffusion coefficient of the order  $10^{-8} \text{ m}^2 \text{ s}^{-1}$  for the nm-sized surfactant molecule in water. The latter timescale (slow motion) was estimated as  $V\rho/a \approx 1 \text{ s}$  for a particle of micrometer radius moving with micrometers  $\text{s}^{-1}$  velocity. These two-time scales were different by two orders of magnitude, which justified the assumption of the quasi-steady-state distribution of the surfactant being established around the particle. The particle was considered as uniformly active, compact heavy sphere near a wall and thus could be analyzed as described elsewhere.<sup>[46-49]</sup> It was assumed here that for these particles the permeability was not significant. Thus, the hydrodynamics was approximated simply by that corresponding to the flow around a compact particle of the same radius  $a$ , but of a reduced mass density (accounting for a fraction  $p$  of the volume of the particle to be of the same density as the fluid).

To summarize, it arrived at the model of a uniformly active, compact, heavy sphere near a wall. The sphere had a constant flux  $K$  as a boundary condition for the chemical activity at its surface. Its chemical activity translated to a hydrodynamic flow  $\mathbf{v}(\mathbf{r})$ , which was incompressible ( $\nabla \cdot \mathbf{v} = 0$ ) and governed by the incompressible Stokes equations:  $\mu \nabla^2 \mathbf{v}(\mathbf{r}) - \nabla p = 0$  (with  $\mu$  the viscosity and  $p$  the pressure), via the boundary conditions of phoretic slip along the particle,  $\mathbf{v}(\mathbf{r} \rightarrow \text{particle}) \rightarrow \nu_p = -b_p \nabla_{\parallel} C$ , and osmotic slip along the wall,  $\mathbf{v}(\mathbf{r} \rightarrow \text{wall}) \rightarrow \nu_w = -b_w \nabla_{\parallel} C$ , where  $b_p$  and  $b_w$  denote the phoretic and osmotic mobilities, respectively. It was noted that the assumption of Stokes flow was well justified for the hydrodynamics of the aqueous solution (density  $\rho = 10^3 \text{ kg m}^{-3}$ , viscosity  $\mu = 10^3 \text{ Pa s}$ ) driven by the chemical activity: the corresponding Reynolds number was estimated to be  $Re < 10^{-5}$  (by using the velocity  $V \approx 1 \text{ } \mu\text{m s}^{-1}$  of typical chemically active Janus particles and the particle radius  $R \approx 1\text{--}10 \text{ } \mu\text{m}$  as a characteristic length scale). Due to the linearity of the Stokes equations, the effects of the phoretically driven flows and those due to the sedimentation driven by the apparent weight, could be accounted for separately and included by linear superposition. Such a model was employed and analyzed previously.<sup>[47-49]</sup> For completeness, detailed calculations are provided in (Section S2-S4 of the Supporting Information) while here it was discussed only a simple, physically insightful, solution based on far-field approximations.

**Theoretical Estimate of  $h_{ac}$ :** For repulsive interactions of the *cis* isomer with the surface of the particle and with that of the wall, the phoretic flows due to the chemical activity were such that they induced an upward motion of the particle with a velocity  $V_a$ . This velocity depended on the distance  $h$  between the center of the particle and the wall: it decreased from a maximum, when the particle was near the wall (i.e., at  $h/a \gtrsim 1$ ), to 0 when the particle was far from the wall (because the system, consisting of a chemically active, spherical particle in a bulk liquid solution, is isotropic). As noted above and detailed in Supporting Information (Section 2), the linearity of the Stokes equations allowed to write the active velocity as the sum of a contribution  $V_p(h)$  due to the phoretic slip along the particle and a contribution  $V_w(h)$  due to the phoretic slip along the wall,

$$V_a(h) = V_p(h) + V_w(h) \quad (5)$$

In a simple, far-field approximation, each of these could be easily rationalized and computed. The first one was the result of the distortion by the wall of the field  $C(\mathbf{r})$ , which far from the wall would be radially symmetric around the uniformly active spherical particle. It could be then seen as the

phoretic response to the density field of the “image” of the particle across the wall; in the first approximation (far field, i.e., particle far from the wall), this was that of a monopolar source of the same strength and located at the mirror image point across the wall. This led to (see the details in the Supporting Information, Section S4) a velocity normal to the wall and into the fluid

$$V_p(h) = -\frac{1}{4}\beta_p V_0 \left(\frac{h_{ac}}{a}\right)^{-2} \quad (6)$$

where  $\beta_p = b_p/|b_p|$  and the characteristic velocity  $V_0$  was given by

$$V_0 := \frac{|b_p|K}{D} := \nu_0 a^n \quad (7)$$

with the second equality factoring out an eventual dependence of  $K$  on the radius  $a$  of the particle (thus  $\nu_0$  is independent of  $a$ ), for example, due to different morphologies of the porous network for smaller and larger particles, respectively.

The contribution of the phoretic slip at the wall follows from the fact that the flow along the wall was radially convergent to the location right underneath the particle and, by incompressibility, it must continue vertically into the bulk. This induced the vertical drift of the particle, which in the first approximation could be taken to be equal to the surface-driven flow evaluated at the center of the particle (in the spirit of Faxen’s law). The far-field calculation of this surface flow, using the results from ref. [45], then led to a velocity normal to the wall and into the fluid

$$V_w(h) = -\frac{1}{2}\beta_w V_0 \left(\frac{h_{ac}}{a}\right)^{-2} \quad (8)$$

where  $\beta_w = b_w/|b_p|$ . For repulsive interactions between the *cis* molecules and the surfaces of the particle and the wall, one had  $b_{p,w} < 0$ , and thus  $\beta_p = -1$  and  $\beta_w < 0$ . Furthermore, since the wall was made of glass and the particles were porous silica, one expected  $b_w \approx b_p$ , thus  $\beta_w \approx -1$ ; in the following estimate, it would simply take  $\beta_w = \beta_p = -1$ .

While the activity-driven motion of the particle was upward, on the other hand the “apparent” (corrected for buoyancy) weight of the particle-induced a downward motion of the particle (sedimentation). The sedimentation velocity  $V_s$  also depended on the distance  $h$  from the wall, and for the model porous particle as described above, was given by:

$$\begin{aligned} V_s(h) &= \frac{\text{apparent weight}}{\text{wall} - \text{corrected Stokes drag}} \\ &= \frac{(4\pi/3)(1-p)(\rho_{\text{SiO}_2} - \rho_{\text{H}_2\text{O}})(a)^3 g}{6\pi\mu a} \gamma_z \left(\frac{h}{a}\right) : \\ &= Ca^2 \gamma_z \left(\frac{h}{a}\right) \end{aligned} \quad (9)$$

where the factor  $(1-p)$  accounted for the part of the volume of the sphere which was made out of silica and displaced fluid (water), the factor  $C$  is a material constant, independent of  $a$ , and the function  $\gamma_z(h/a)$  denotes the wall-correction of the Stokes motility (the inverse of the drag factor) for the motion of a sphere in the direction normal to the wall. The expression for  $\gamma_z(h/a)$  as a series in  $h/a$  (Supporting Information, Section S4) is a well-known result of Brenner.<sup>[50,51]</sup> In the far field approximation,  $\gamma_z = 1$ .

The competition between the downward motion with  $V_s(h)$  and the upward motion with  $V_a(h)$  could give rise to a mechanical equilibrium state at a height  $h_{ac}$  for which  $V_a(h_{ac}) = V_s(h_{ac})$ ; this provided an equation that could, in general, be solved numerically to determine the height  $h_{ac}$  of the

active particle of radius  $a$ . In the far field, however, by collecting the results above the equation for  $(h_{ac}/a)$  takes the very simple form:

$$Ca^2 = -\frac{1}{4}(\beta_p + 2\beta_w) V_0 \left(\frac{h_{ac}}{a}\right)^{-2} \quad (10)$$

from which one infers  $h_{ac}/a \approx a^{-1}$  (assuming that  $K$ , and thus  $V_0$ , is independent of  $a$ ). This could be tested by comparing with the behavior of the ratio of the speeds in the external flow in the illuminated and the dark regions, respectively. From Equations (3) and (4), in the far field limit ( $h/a \gg 1$ ) one predicts  $U_l/U_d \approx h_{ac}/a$ , and thus, by combining with the result above,  $U_l/U_d \approx a^{-1}$ . This seems compatible with the behavior shown in Figure 3b, which was remarkable in view of the strong approximations involved in the far-field analysis.

## Supporting Information

Supporting Information is available from the Wiley Online Library or from the author.

## Acknowledgements

M.B. and M.S. contributed equally to this work. M.B. acknowledges financial support from the National German Science Foundation (DFG) through the grant BE 7745/1-1. M.N.P. acknowledges financial support by the Spanish Junta de Andalucía through grant US-1380729, the Spanish Ministerio de Universidades through a María Zambrano funded by Ministerio de Universidades and NextGenerationEU, US-1380729 funded by US/JUNTA/FEDER-UE, ProyExcel\_00505 funded by Junta de Andalucía, and PID2021-126348N funded by MCIN/AEI/10.13039/501100011033/ and ERDF A way of making Europe.

Open access funding enabled and organized by Projekt DEAL.

## Conflict of Interest

The authors declare no conflict of interest.

## Data Availability Statement

The data that support the findings of this study are available in the supplementary material of this article.

## Keywords

azobenzene containing surfactants, colloids, light-induced motion, local light driven diffusioosmosis, particle separation

Received: January 12, 2023

Revised: March 11, 2023

Published online: April 29, 2023

- [1] T.-S. Wong, S. H. Kang, S. K. Y. Tang, E. J. Smythe, B. D. Hatton, A. Grinthal, J. Aizenberg, *Nature* **2011**, 477, 443.
- [2] R. H. Bishop, *Mechatronics: An Introduction*, (Ed: T. Francis), Taylor & Francis, Boca Raton, FL, USA **2006**, p. 312.
- [3] L. Scarabelli, D. Vila-Liarte, A. Mihi, L. M. Liz-Marzán, *Acc. Mater. Res.* **2021**, 2, 816.
- [4] Z. Cai, Z. Li, S. Ravaine, M. He, Y. Song, Y. Yin, H. Zheng, J. Teng, A. Zhang, *Chem. Soc. Rev.* **2021**, 50, 5898.

- [5] F. Bian, L. Sun, L. Cai, Y. Wang, Y. Wang, Y. Zhao, *Small* **2020**, *16*, 1903931.
- [6] P. Sajeesh, A. K. Sen, *Microfluid. Nanofluid.* **2014**, *17*, 1.
- [7] J. Mc. Murry, *Organic chemistry: with biological applications*, 2nd ed., Brooks/Cole, Belmont, CA, USA **2011**.
- [8] P. J. Marinaccio, R. W. Monroe, R. V. Repetti, *USA 4* **1989**, *888*, 115.
- [9] M. Cheryan, *Ultrafiltration Handbook*, Technomic Publishing Co, Lancaster, PA, USA **1986**.
- [10] A. Dalili, E. Samieib, M. A. Hoorfar, *Analyst* **2019**, *144*, 87.
- [11] Y. Gou, Y. Jia, P. Wang, C. Sun, *Sensors* **2018**, *18*, 1762.
- [12] C. W. Shields IV, C. D. Reyes, G. P. López, *Lab Chip* **2015**, *15*, 1230.
- [13] C. P. Pilkington, J. M. Seddon, Y. Elani, *Phys. Chem. Chem. Phys.* **2021**, *23*, 3693.
- [14] W. Tang, S. Zhu, L. Zhu, J. Yang, N. Xiang, *Lab Chip* **2020**, *20*, 3485.
- [15] J. Ma, Y. Wang, J. Liu, *Micromachines* **2017**, *8*, 255.
- [16] M. Yamada, M. Nakashima, M. Seki, *Anal. Chem.* **2004**, *76*, 5465.
- [17] L. R. Huang, E. C. Cox, R. H. Austin, J. C. Sturm, *Science* **2004**, *304*, 987.
- [18] N. Convery, N. Gadegaard, *Micro Nano Eng.* **2019**, *2*, 76.
- [19] T. V. Nizkaya, E. S. Asmolov, J. Harting, O. I. Vinogradova, *Phys. Rev. Fluids* **2020**, *5*, 014201.
- [20] E. S. Asmolov, A. L. Dubov, T. V. Nizkaya, J. Harting, O. I. Vinogradova, *J. Fluid Mech.* **2018**, *840*, 613.
- [21] T. Torimoto, N. Yamaguchi, Y. Maeda, K. Akiyoshi, T. Kameyama, T. Nagai, T. Shoji, H. Yamane, H. Ishihara, Y. Tsuboi, *npg Asia Mater.* **2022**, *14*, 64.
- [22] B. Abecassis, Cottin-Bizonne, C. Cottin-Bizonne, C. Ybert, A. Aidari, L. Bocquet, *Nat. Mater.* **2008**, *7*, 785.
- [23] D. Feldmann, S. R. Maduar, M. Santer, N. Lomadze, O. I. Vinogradova, S. Santer, *Sci. Rep.* **2016**, *6*, 36443.
- [24] J. Eastoe, A. Vesperinas, *Soft Matter* **2005**, *1*, 338.
- [25] Y. Zakrevskyy, J. Roxlau, G. Brezesinski, N. Lomadze, S. Santer, *J. Chem. Phys.* **2014**, *140*, 044906.
- [26] H. Rau, n *Photochemistry and Photophysics*, (Ed.: J. F. Rabek), CRC Press, Inc, Boca Raton, FL, USA **1990**.
- [27] M. Montagna, O. Guskova, *Langmuir* **2018**, *34*, 311.
- [28] S. Santer, *J. Phys. D Appl. Phys.* **2018**, *51*, 013002.
- [29] S. Marbach, L. Bocquet, *Chem. Soc. Rev.* **2019**, *48*, 3102.
- [30] J. C. T. Eijkel, A. van den Berg, *Chem. Soc. Rev.* **2010**, *39*, 957.
- [31] J. L. Anderson, D. C. Prieve, *Langmuir* **1991**, *7*, 403.
- [32] J. L. Anderson, M. E. Lowell, D. C. Prieve, *J. Fluid Mech.* **1982**, *117*, 107.
- [33] C. Lee, C. Cottin-Bizonne, R. Fulcrand, L. Joly, C. Ybert, *J. Phys. Chem. Lett.* **2017**, *8*, 478.
- [34] P. Arya, M. Umlandt, J. Jelken, D. Feldmann, N. Lomadze, E. S. Asmolov, O. I. Vinogradova, S. A. Santer, *Eur. Phys. J. E* **2021**, *44*, 50.
- [35] D. Feldmann, P. Arya, T. Y. Molotilin, N. Lomadze, A. Kopyshv, O. I. Vinogradova, Santer, S, *Langmuir* **2020**, *36*, 6994.
- [36] A. Sharma, M. Bekir, N. Lomadze, S. Santer, *Macromol. Chem.* **2021**, *26*, 19.
- [37] P. Arya, J. Jelken, D. Feldmann, N. Lomadze, S. Santer, *J. Chem. Phys.* **2020**, *152*, 194703.
- [38] P. Arya, D. Feldmann, A. Kopyshv, N. Lomadze, S. Santer, *Soft Matter* **2020**, *16*, 1148.
- [39] M. Umlandt, D. Feldmann, E. Schneck, S. A. Santer, M. Bekir, *Langmuir* **2020**, *36*, 14009.
- [40] A. Sharma, M. Bekir M, N. Lomadze N, S-H. Jung, A. Pich, S. Santer, *Langmuir* **2022**, *38*, 6343.
- [41] M. Bekir, A. Sharma, M. Umlandt, N. Lomadze, S. Santer, *Adv. Mater. Interfaces* **2022**, *2102395*.
- [42] P. Arya, J. Jelken, N. Lomadze, S. Santer, M. Bekir, *J. Chem. Phys.* **2020**, *152*, 024904.
- [43] M. Frenkel, P. Arya, E. Bormachenko, S. Santer, *J. Colloid Interface Sci.* **2021**, *586*, 866.
- [44] D. Dumont, T. V. Galstian, S. Senkow, A. M. Ritcey, *Mol. Cryst. Liq. Cryst.* **2002**, *375*, 341.
- [45] A. J. Goldman, R. G. Cox, H. Brenner, *Chem. Eng. Sci.* **1967**, *22*, 653.
- [46] R. Golestanian, T. B. Liverpool, A. Ajdari, *New J. Phys.* **2007**, *9*, 126.
- [47] P. Margaretti, M. N. Popescu, S. Dietrich, *Soft Matter* **2018**, *14*, 1375.
- [48] D. P. Singh, W. E. Uspal, M. N. Popescu, L. G. Wilson, P. Fischer, *Adv. Funct. Mater.* **2018**, *28*, 1706660.
- [49] A. Domínguez, P. Margaretti, M. N. Popescu, S. Dietrich, *Phys. Rev. Lett.* **2016**, *116*, 078301:1.
- [50] J. Happel, H. Brenner, *Low Reynolds Number Hydrodynamics*, Prentice-Hall, Englewood Cliffs, NJ, USA **1965**.
- [51] H. Brenner, *Chem. Eng. Sci.* **1961**, *16*, 242.